NANO · MICRO small
www.small-journal.com

# Bacteria-Targeted MRI Probe-Based Imaging Bacterial Infection and Monitoring Antimicrobial Therapy In Vivo

*Linyao Li, Peilin Gu, Mengqi Hao, Xiaoli Xiang, Yuting Feng, Xiaokang Zhu, Yang Song, and Erqun Song**

**Despite the significant advances of imaging techniques nowadays, accurate diagnosis of bacterial infections and real-time monitoring the efficacy of antibiotic therapy in vivo still remain huge challenges. Herein, a self-assembling peptide (FFYEGK) and *vancomycin* (*Van*) antibiotic molecule co-modified gadolinium (Gd) MRI nanoaggregate probe (GFV) for detecting *Staphylococcus aureus* (*S. aureus*) infection in vivo and monitoring the treatment of *S. aureus*-infected myositis by using daptomycin (*Dap*) antibiotic as model are designed and fabricated. The as-prepared GFV probe bears *Van* molecules, making itself good bacteria-specific targeting, and the peptide in the probe can enhance the longitudinal relaxivity rate ($r_1$) after self-assembly due to the $\pi$–$\pi$ stacking. The study showed that, based on the GFV probe, bacterial infections and sterile inflammation can be discriminated, and as few as $10^5$ cfu *S. aureus* can be detected in vivo with high specificity and accurately. Moreover, the $T_1$ signal of GFV probe at the *S. aureus*-infected site in mice correlates with the increasing time of *Dap* treating, indicating the possibility of monitoring the efficacy of antibacterial agents for infected mice based on the as proposed GFV probe. This study shows the potential of GFV probe for diagnosis, evaluation, and prognosis of infectious diseases in clinics.**

## 1. Introduction

Bacterial infections have been a major cause of morbidity and mortality globally[1,2] due to the substantially increased incidence of infectious diseases,[3,4] increased susceptibility to infections,[5,6] and increased drug-resistance of bacteria.[7,8] Gold standard detection approaches for bacterial infections based on tissue biopsies and culture of causative organisms are invasive, time-consuming, and cannot detect early-stage infections.[9,10] In recent years, various diagnostic imaging modalities in vivo, including ultrasound (US),[8,11,12] photoacoustic tomography (PAT),[13–15] magnetic resonance imaging (MRI),[16–19] computed tomography (CT),[20,21] positron emission tomography (PET),[22,23] and fluorescence/bioluminescence imaging (FI/BLI),[24–30] have been applied to study bacterial infections. However, most of these imaging methods are not feasible to distinguish between bacterial infections and inflammations in vivo, and have not been applied to monitor efficacy of anti-infectious therapy. Thus, there is an urgent need for an imaging technology that can specifically and noninvasively detect pathogens in vivo and monitor the progress of bacterial infection treatment.

MRI has been widely used to detect acute injury, musculoskeletal disease, and central nervous system infections due to its excellent intrinsic soft tissue contrast, superior spatial resolution, and unlimited tissue penetration depth.[31] However, the development of targeted MRI contrast agents for bacterial infections has not been earnestly valued, and currently there is no bacteria-targeted MRI contrast agents available for routine clinical diagnosis. Renshaw's group had developed biocompatible super-paramagnetic iron oxide nanoparticles conjugated with *Mycobacterium tuberculosis* (Mtb) antibody to target and detect Mtb infection in vivo.[32] Hu's group has specially monitored Gram-positive and Gram-negative bacterial cells with gadolinium (Gd)-based bacteria-specific targeting MRI contrast agent probe by conjugating an aminoglycoside antibiotic.[17] Despite the improved specificity, the low sensitivity of bacterial imaging limited their clinical application. Therefore, this calls for the development of a sensitive and specific MRI strategy to identify and localize bacterial infections.

Recently, the strategy of "self-assembly of supramolecular assemblies" has been applied for bacterial detection due to the enhanced signals.[13,33,34] Taking the self-assembling of peptide, Liu's group demonstrated a sensitive and selective detection of Gram-positive bacteria in vivo in myositis and pneumonia models based on fluorescent and isotopic signal.[34] Inspired by the previous work, we designed and synthesized a new $T_1$-weighted MRI probe (GFV), composed of $Gd^{3+}$ as a $T_1$ signaling unit, *Van* as a target ligand, and self-assembling peptide

L. Y. Li, P. L. Gu, M. Q. Hao, X. L. Xiang, Y. T. Feng, X. K. Zhu, E. Q. Song
Key Laboratory of Luminescence Analysis and Molecular Sensing
College of Pharmaceutical Sciences
Southwest University
Chongqing 400715, China
E-mail: eqsong@swu.edu.cn
Y. Song
State Key Laboratory of Environmental Chemistry and Ecotoxicology
Research Center for Eco-Environmental Sciences
CAS
Beijing 100085, China

The ORCID identification number(s) for the author(s) of this article can be found under https://doi.org/10.1002/smll.202103627.

**DOI: 10.1002/smll.202103627**

 

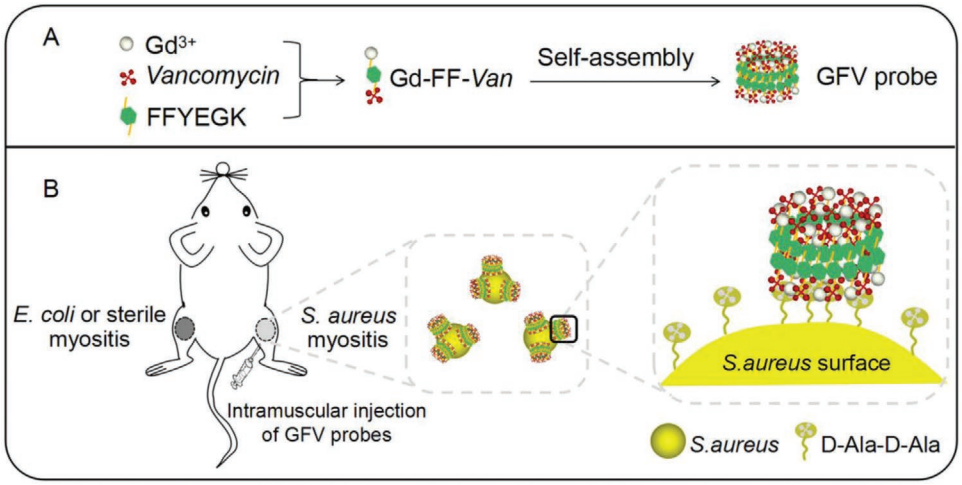


**Scheme 1.** Schematics of A) the preparation of multifunctional GFV probe and B) bacterial infection imaging in vivo based on GFV probe.

FFYEGK (FF) for signal enhancement, which could specifically and sensitively detect *Staphylococcus aureus* (*S. aureus*) infection in mouse myositis model (as shown in **Scheme 1**). Due to the excellent $\pi$–$\pi$ stacking of "Phenylalanine–Phenylalanine," the monomer of GFV probe (Gd-FF-*Van*) could self-assemble to form nanoaggregate probe which have a high longitudinal relaxivity rate ($r_1$). This study showed that GFV probe could specifically image *S. aureus* at the site of infection owing to its specific binding to the cell walls of *S. aureus* through hydrogen-bonding interactions between *Van* and the D-alanyl-D-alanine dipeptide extending from the cell wall,[35] and sensitively image *S. aureus* due to its high $r_1$ value. Thus, this proposed noninvasive MR imaging strategy could distinguish between bacterial infections from sterile inflammations. Moreover, this work had successfully monitored the efficacy of *Daptomycin* (*Dap*) for *S. aureus* infected mouse models. The specific and sensitive detection of *S. aureus* infection in vivo based on the as-proposed GFV probe demonstrated the potential applicability of this noninvasive imaging strategy in diagnosis of bacterial infections and real-time monitoring efficacy of antibiotic treatment in clinic.

## 2. Results and Discussion

### 2.1. Synthesis and Characterization of GFV Probe

In this study, Gd-FF-*Van*, as the monomer of GFV probe, was synthesized according to the procedures illustrated in Figure S1 (Supporting Information) and consists of a paramagnetic $Gd^{3+}$ chelate as $T_1$ signaling unit, *Van* as a target ligand to *S. aureus*, and a hydrophobic dipeptide Phenylalanine–Phenylalanine (FF) linker promoting self-assembly. In order to verify the self-assembly of Gd-FF-*Van*, Gd-GG-*Van* as a control compound was synthesized according to the same procedure as that for Gd-FF-*Van*, only replacing FF with glycine–glycine (GG). Detailed synthesis procedures were provided in the Supporting Information, and their structures were confirmed by $^1$H NMR spectroscopy and FTICR-MS (Figures S2–S6, Supporting Information).

Due to the intermolecular interactions (hydrophobic interactions and $\pi$–$\pi$ stacking) of FF, Gd-FF-*Van* (when the concentration of Gd-FF-*Van* is higher than their critical aggregation concentration about 74 $\mu$g mL$^{-1}$, Figure S7, Supporting Information) self-assembled to spherical nanoparticles (as GFV probe) with an average size of 50 nm as shown in **Figure 1**A while Gd-GG-*Van* exhibited amorphous morphologies (Figure 1B). The ultraviolet–visible (UV–vis) absorption spectra show that the GFV probe had the characteristic peak at 280 nm of *Van* (Figure S8, Supporting Information). The longitudinal relaxivity rate ($r_1$) of GFV probe (22.32 mM$^{-1}$ s$^{-1}$) was much higher than that of Gd-GG-*Van* (7.47 mM$^{-1}$ s$^{-1}$), Gd-FF (5.77 mM$^{-1}$ s$^{-1}$), and Gd-GG (5.19 mM$^{-1}$ s$^{-1}$) under a 0.5 T external magnetic field (Figure 1C), and was much higher than that of clinical Gd-based complex,[36,37] indicating that GFV probe had better $T_1$ contrast efficacy as MRI contrast agents. The high $r_1$ value of GFV probe might attribute to its specific nanoaggregated structural characteristics which would restrict molecular rotation and prolong the tumbling time of Gd-chelates.[38]

### 2.2. The Specific Recognition of GFV Probe with Bacteria

First, we investigated the specific recognition of GFV probe to *S. aureus* in vitro. As shown in Figure S9A (Supporting Information), $T_1$ relaxation times of *S. aureus* incubated with GFV probe were shorter than that incubated with Gd-GG-*Van*, Gd-FF, and Gd-GG, while $T_1$ relaxation times of *E. coli* incubated with GFV probe, Gd-GG-*Van*, Gd-FF, and Gd-GG showed no obvious difference, which were consistent with their $T_1$-weighted MR images shown in Figure S9B (Supporting Information). Both the $T_1$ relaxation times and $T_1$-weighted MR image results demonstrate the as-prepared GFV probe has high specificity for *S. aureus*. Then its feasibility of targeted imaging bacterial infections in vivo was evaluated by employing the *S. aureus*-infected myositis mice model (Figure S10, Supporting Information). Prior to perform the assay in vivo, the background $T_1$ signal of the model was assessed. It was found that the $T_1$ signal at the infection site showed no significantly difference from that at the normal tissue site, indicating that the $T_1$ signal from the infected site would not

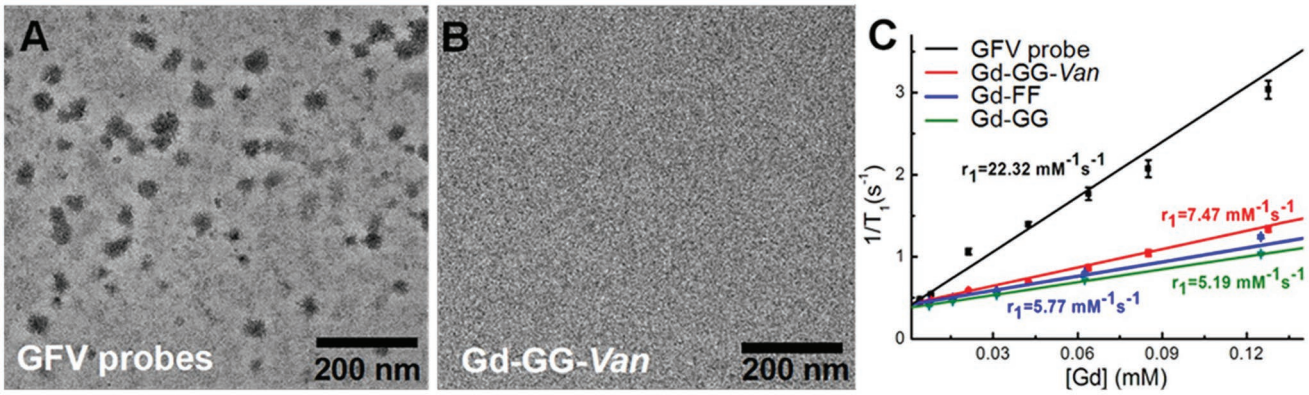


**Figure 1.** Typical TEM images of A) GFV probes and B) Gd-GG-*Van*. C) Values of $1/T_1$ of GFV probe, Gd-GG-*Van*, Gd-FF, and Gd-GG versus Gd concentration.

interfere with the GFV probe's signals (Figure S11, Supporting Information). As shown in Figure S12 (Supporting Information), the MRI signal of GFV probe could not be detected at the *E. coli*-infected site after 4 h while the *S. aureus*-infected site still had an obvious NMR signal, suggesting that the imaging time point of 4 h after intramuscular injection of probes is suitable for detecting *S. aureus* in vivo. Then the specificity of GFV probe for detecting *S. aureus* in vivo was verified through MR imaging of *S. aureus*-infected induced myositis in the left thigh of mice and *E. coli* (**Figure 2**A) or $SiO_2$ (Figure 2B)-induced myositis in the right thigh of mice after intramuscular injection of GFV probe, Gd-GG-*Van* (Figure 2C) or Gd-FF (Figure 2D). As shown in Figure 2A,B, after treated with GFV probe for 4 h, those mice exhibited higher MR intensity around the *S. aureus*-induced infection sites than that of *E. coli* or $SiO_2$-induced myositis sites. And the *S. aureus*-infected mice models treated with Gd-GG-*Van* (Figure 2C) and Gd-FF (Figure 2D) for after 4 h, they showed lower MRI signal than that treated with GFV probe. And all the relatively enhanced MR signal intensity (SI) corresponding to Figure 2 were shown in Figure S13 (Supporting Information). Therefore, those results proved the specificity of GFV probe for detecting *S. aureus* in vivo.

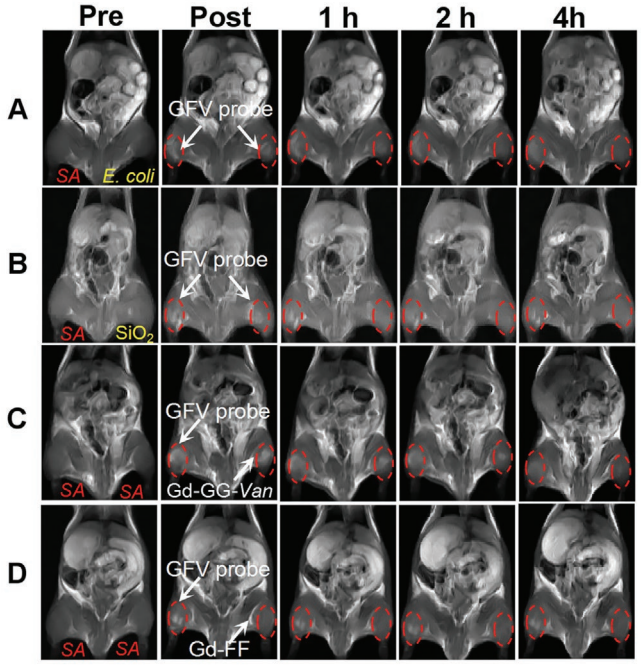


**Figure 2.** $T_1$-weighted MR images of *S. aureus*-induced myositis mice in the left thigh muscle, A) *E. coli*-induced myositis or B) $SiO_2$ NPs-induced sterile infection in the right thigh muscle injecting GFV probe (0.01 mmol $kg^{-1}$ $Gd^{3+}$); *S. aureus*-induced infected mice with myositis in the left thigh muscle injecting GFV probe and in the right thigh muscle injecting C) Gd-GG-*Van* and D) Gd-FF. Images were acquired before (Pre), Post, 1, 2, and 4 h after injection, using TE/TR = 20/300 ms at 0.5 T.

Moreover, to further confirm the colocalization of GFV probe and bacterial infected site in vivo, near-infrared dye (Cy5) prestained *S. aureus* (Cy5-*SA*), and *E. coli* (Cy5-*E. coli*) were employed to construct myositis mice model. After treated with GFV probe, the as-constructed mice models were subjected to fluorescence imaging and $T_1$-weighted MRI, respectively. As shown in **Figure 3**A, the left and right thigh muscles of mice had strong fluorescent signal at the site of bacterial injection, indicating that the bacteria localized at the site of bacterial injection rather than elsewhere. After intramuscularly injecting of GFV probe for 4 h, the Cy5-*SA* infected site showed higher MRI signal than that of Cy5-*E. coli* infected site (Figure 3B and Figure S14, Supporting Information). All the above-mentioned results demonstrated that the GFV MRI probes could specifically target and localize *S. aureus* at the infection site in vivo and have high effectiveness for MRI visualization.

### 2.3. Detection of *S. aureus* Infection in Vivo

Before applying GFV probe to detect *S. aureus* in vivo, the cytotoxicity of GFV probe to *S. aureus* and cells was evaluated and the biocompatibility of probe was examined by pathologies through the hematoxylin and eosin (H&E) assay. As shown in Figure S15 (Supporting Information), the proliferation of *S. aureus* was not significantly affected by the presence of GFV probe, and the in vitro cytotoxicity study indicated that GFV probe showed little toxicity toward RAW 264.7 cells (Figure S16, Supporting Information). H&E assays of the main organs (heart, liver, spleen, lung, kidney and thigh muscle) of GFV probe administrated mice indicated no obvious toxicity of GFV

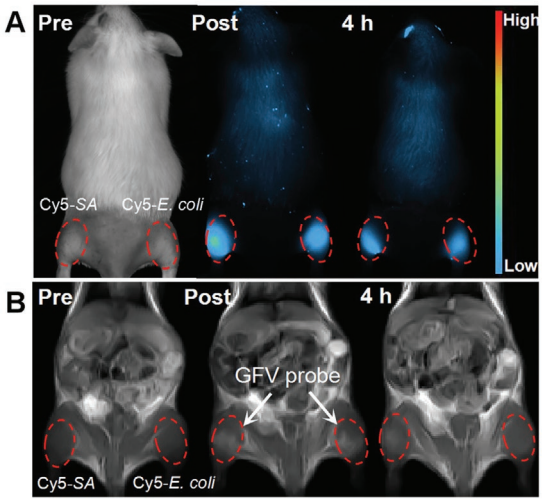


**Figure 3.** A) In vivo near-infrared fluorescence (NIRF) images and B) $T_1$-weighted MR images of infected mice with Cy5-labeled *S. aureus* in the left thigh muscle, Cy5-labeled *E. coli* in the right thigh muscle treated with GFV probe (0.01 mmol $kg^{-1}$ $Gd^{3+}$) at 4 h postinjection.

probe to the mice (Figure S17, Supporting Information). After the dosage of GFV probe was optimized (Figure S18, Supporting Information), the detection limit of target *S. aureus* by GFV probe in vivo was studied. Specifically, different concentrations of *S. aureus* ($10^3$, $10^4$, $10^5$, $10^6$, $10^7$, and $10^8$ cfu) were intramuscularly injected into thigh muscle of mice, and after 24 h, GFV probes were injected into the site of *S. aureus* infected, followed acquiring $T_1$-weighted MRI images. As shown in **Figure 4** and Figure S19 (Supporting Information), the enhanced MRI signal was correlated with the concentration of *S. aureus,* and as few as $10^5$ cfu of *S. aureus*-induced myositis could show discernable MRI signal of GFV probe.

Therefore, the number of *S. aureus* at the infection site could be real-time monitored through MRI, which is conducive to monitoring of antimicrobial therapy efficacy and avoiding the abuse of antibiotics in clinical.

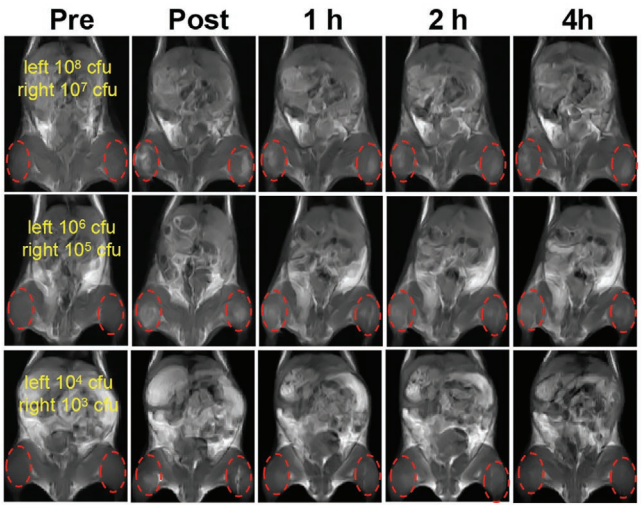


**Figure 4.** $T_1$-weighted MR images of mice infected with various concentrations of *S. aureus* in the thigh muscle before and after intramuscular injection of GFV probe (0.01 mmol $kg^{-1}$ $Gd^{3+}$).

### 2.4. Monitoring Antimicrobial Therapy of Dap to *S. aureus* Infection with GFV Probe

Prior to investigate the capability of GFV probe to monitor the efficacy of antibiotic treatment in vivo, the curative effect of *Dap* to *S. aureus* in vivo was studied.[39] *Dap* treated *S. aureus* infection for different days (1, 2, 3, 4, 5, 6, and 7 d) were determined by counting bacterial colonies formed on the LB-agar plates derived from the homogenized tissue from the infected sites of mice. Figure S20 (Supporting Information) showed that the number of *S. aureus* at the infected site decreased with increasing in days of administration of *Dap*, which indicated that continuous administration of *Dap* could effectively treat *S. aureus* infectious disease, and after 7 d of *Dap* treatment, the number of bacteria at the infected site was about $2 \times 10^5$ cfu, which was within the detection range of the GFV probe. Then GFV probe was employed to monitor efficacy of *Dap* to *S. aureus* infection in vivo. After treated with *Dap* for different days, the *S. aureus*-infected mice were intramuscularly injected with GFV probe for MR imaging (Figure S21, Supporting Information), following excised and homogenized, and the number of bacteria was determined by standard plate count method. According to the data shown in **Figure 5**, the decrease relatively enhanced MR SI at the *S. aureus* infected site (Figure 5A) was correlated with the decreased number of *S. aureus* at the infected site as the increased days of administration of *Dap* (Figure 5B and Figure S22, Supporting Information). These results demonstrated the potential of the as-proposed MR imaging-based strategy to monitor the efficacy of antimicrobial therapy in vivo, which may be of considerable application potential in clinic.

## 3. Conclusion

In summary, this work demonstrated a feasible strategy to accurately and specifically image bacteria in vivo and to monitor the antimicrobial efficacy of antibiotics with bacteria-targeted MRI probes consisting of $T_1$ signal molecule ($Gd^{3+}$), a target ligand (*Van*), and self-assembling peptide (FF). Thanks to the ability of *Van* to specifically target bacteria and the self-assembly of Gd-FF-*Van* to form GFV probe with high $r_1$ relaxivity, *S. aureus* could be specifically and precisely detected by MR imaging with GFV probes in vivo. Additionally, the as-proposed GFV MRI probe could monitor the efficacy of antimicrobial therapy of *S. aureus* infections through estimating of the number of *S. aureus* loading in the infected site timely, indicating its great potential for assist physicians in providing effective treatment options for bacterial infectious diseases.

## 4. Experimental Section

*Materials and Apparatus*: Cystamine dihydrocholoride, tris(2-carboxyethyl)phosphine hydrochloride (TCEP), *O*-(benzotriazol-1-yl)-*N*, *N*, *N*', *N*'- tetramethyluronium hexafluorophosphate (HBTU),

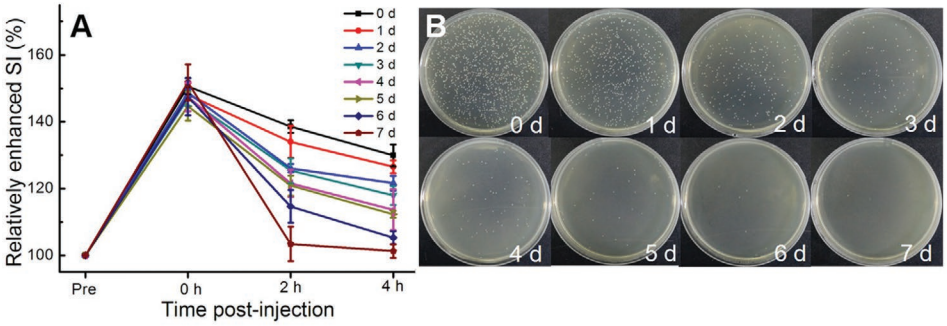


**Figure 5.** A) Relatively enhanced MR SI and B) photographs of the cultured agar plates ($10^4$ times dilution) of the *S. aureus* at infected site treated with *Dap* for different days (1, 2, 3, 4, 5, 6, and 7 d) with GFV probe (0.01 mmol $kg^{-1}$ $Gd^{3+}$).

diisopropylethylamine (DIEA), and other chemicals were purchased from Aladdin Industrial Inc. (Shanghai, China). *Daptomycin* (*Dap*) was purchased from Yuanye Bio-technology Co., Ltd. (Shanghai, China). Tryptone soy broth (TSB) was obtained from Solarbio Science & Technology Co., Ltd. (Beijing, China). *Vancomycin* hydrochloride, the peptides DOTA-FFYEGK-Mal, and DOTA-GGYEGK-Mal were synthesized by Shanghai Sangon Biological Science & Technology Company (Shanghai, China). *S. aureus* (ATCC 29213) was obtained from China General Microbiological Culture Collection Center. *Escherichia coli* O78 (*E. coli*) was obtained from the China Center of Industrial Culture Collection. Male Kunming mice (5 weeks, ≈25 g) were purchased from SJA Laboratory Animal Co. Ltd. (Hunan, China). All animal experiments in this study were approved by the Institutional Animal Care and Use Committee (IACUC) of the Southwest University.

$^1$H NMR spectra were taken on a Bruker Advance 430 MHz spectrometer (Bruker Co., Ltd., Switzerland). Fourier-transform ion cyclotron resonance mass spectrometer (FTICR-MS; Varian, Inc., America) spectrometric analyses was used to characterize the compounds. HPLC was performed at LC-2130 HPLC (Hitachi, Japan) system using a $C_{18}$ RP column with MeOH (0.05% of TFA) and water (0.05% of TFA) as mobile phases. Morphology and microscopic structure of probes were characterized using a transmission electron microscope (TEM) (JEM 1200EX, JEOL Ltd.). Hydrodynamic diameter was measured using a Malvern Zetasizer Nano ZS ZEN3600 instrument (Malvern Instruments, United Kingdom). Near-infrared fluorescence (NIRF) images were obtained by using Smart Imaging System (NEWTON 7.0, France). MRI tests were conducted on the 0.5 T small animal MR scanner (MesoMR23, China).

*Bacteria and Cell Culture*: *S. aureus* and *E. coli* were grown in TSB medium at 37 °C. The concentration of bacteria was measured by the bacterial turbidimeter (WGZ-2XJ, China). RAW 264.7 cells were cultured at 37 °C and 5% $CO_2$ in Dulbecco's modified Eagle's medium (DMEM) supplemented with 10% fetal bovine serum (FBS).

*Synthesis of MRI Imaging Probes*: Dimeric vancomycin (bis-*Van*) and sulfhydrylation *vancomycin* (SH-*Van*) were synthesized according to the published procedures.[34,40] Then *Van* modified DOTA-peptide derivative DOTA-FFYEGK-*Van* (DOTA-FF-*Van*) and DOTA-GGYEGK-*Van* (DOTA-GG-*Van*) were synthesized by Michael addition reaction between the sulfhydryl of SH-*Van* and the maleimide of DOTA-FF and DOTA-GG. In a typical synthesis, 2 mg of SH-*Van* and 1 mg of DOTA-FF or DOTA-GG were dissolved in 1 mL of anhydrous DMF, and subsequently 10 µL of triethylamine was added. After stirred at room temperature for 24 h, the mixture was purified by dialysis and lyophilized to provide DOTA-FF-*Van* and DOTA-GG-*Van*. Finally, the self-assembling probe (GFV) and Gd-GG-*Van* were obtained through the chelation of $Gd^{3+}$ with DOTA group of DOTA-FF-*Van* and DOTA-GG-*Van*. Detailed information on the synthesis and characterization of above compounds is described in the Supporting Information.

*Measurement of MR Relaxivity of As-Prepared Compounds*: The $r_1$ relaxivities of GFV probe and control agents (Gd-GG-*Van*, Gd-FF, and Gd-GG) were measured on a 0.5 T MesoMR NMR Analyzing system at 37 °C. A series of GFV probe, Gd-GG-*Van*, Gd-FF, and Gd-GG aqueous solution samples with different concentration were performed to $T_1$ measurement, and then the $r_1$ values were obtained by analyzing the slopes of the fit lines of relaxation rates ($1/T_1$) versus the concentrations (mM) of $Gd^{3+}$.

*Establishment of Infection Models in Mice*: The bacterial myositis models of mice were established by intramuscularly injecting $1 \times 10^8$ cfu of *S. aureus* and $1 \times 10^8$ cfu of *E. coli* into the left and right hind legs, respectively, while the sterile inflammation models were created by injecting silica nanoparticles ($SiO_2$ NPs, 100 nm, 20 mg $mL^{-1}$) into the leg muscle of mice. After 24 h, MR images of those models were acquired, and the infected thigh muscles were cut for H&E assay to validate infection models.

*Specificity of $T_1$-Weighted Imaging Bacterial Infections with GFV Probe In Vivo*: After the bacterial myositis models of mice were established, those mice were anaesthetized by administration of 0.1 mL of chloral hydrate (10 wt%) through intraperitoneal injection, and then GFV probe, Gd-GG-*Van*, and Gd-FF were respectively injected into the site of infection at a dose of 0.01 mmol $Gd^{3+}$ per kg of mice body weight, and representative $T_1$-weighted MRI images were collected at the desired time points (0, 1, 2, 4 h). Each group was conducted with three mice. The detailed $T_1$-weighted MR imaging parameters were as follows: repetition time (TR) = 300 ms, echo time (TE) = 20 ms, field of view = 100 × 100 $mm^2$, matrix size = 256 × 192, number of slices = 1, slice thickness = 17 mm, flip angle = 90°, and averages = 8. The SI was obtained through analyzing regions of interest (ROIs) in the images, and the relatively enhanced SI was evaluated according to the following equation: relatively enhanced SI = $(SI_{post}/SI_{pre}) \times 100\%$, where $SI_{pre}$ and $SI_{post}$ stand for the signal intensity before and after injection of probes.

*Monitoring Therapeutic of Dap to S. aureus Infected Mouse with GFV Probe*: A suspension of *S. aureus* ($10^8$ cfu) was injected into the left thigh muscle of mice, and infectious mice were obtained after 24 h. Then those mice were injected with *Dap* via the tail vein (30 mg $kg^{-1}$, every 24 h for 7 d), and control mice received saline instead of *Dap*. After administration of *Dap* for 24 h, the mouse was injected with GFV probes at the *S. aureus* infected site and $T_1$-weighted MRI images were obtained from the MRI scanner at different points in time (0, 1, 2, 4 h). After imaging those mice, the infected muscles of mice were extracted, weighted and homogenized, and the number of bacteria was determined by plate counting.

## Supporting Information

Supporting Information is available from the Wiley Online Library or from the author.

## Acknowledgements

This work was supported by the National Natural Science Foundation of China (21974110 and 21976145).

 

## Conflict of Interest

The authors declare no conflict of interest.

## Data Availability Statement

Research data are not shared.

## Keywords

bacterial infection, imaging, in vivo, monitoring, MRI probe

Received: June 21, 2021
Revised: July 24, 2021
Published online:

[1] S. Piano, V. Singh, P. Caraceni, R. Maiwall, C. Alessandria, J. Fernandez, E. C. Soares, D. J. Kim, S. E. Kim, M. Marino, J. Vorobioff, R. D. R. Barea, M. Merli, L. Elkrief, V. Vargas, A. Krag, S. P. Singh, L. A. Lesmana, C. Toledo, S. Marciano, X. Verhelst, F. Wong, N. Intagliata, L. Rabinowich, L. Colombato, S. G. Kim, A. Gerbes, F. Durand, J. P. Roblero, K. R. Bhamidimarri, T. D. Boyer, M. Maevskaya, E. Fassio, H. S. Kim, J. S. Hwang, P. Gines, A. Gadano, S. K. Sarin, P. Angeli, *International Club of Ascites Global Study Group, Gastroenterology* **2019**, *156*, 1368.
[2] D. Sun, X. Pang, Y. Cheng, J. Ming, S. J. Xiang, C. Zhang, P. Lv, C. C. Chu, X. L. Chen, G. Liu, N. F. Zheng, *ACS Nano* **2020**, *14*, 2063.
[3] D. C. Angus, W. T. Linde-Zwirble, J. Lidicker, G. Clermont, J. Carcillo, M. R. Pinsky, *Crit. Care Med.* **2001**, *29*, 1303.
[4] C. J. Palestro, C. Love, T. T. Miller, *Cell. Microbiol.* **2007**, *9*, 2323.
[5] S. Daghighi, J. Sjollema, H. C. van der Mei, H. J. Busscher, E. T. J. Rochford, *Biomaterials* **2013**, *34*, 8013.
[6] S. Veerachamy, T. Yarlagadda, G. Manivasagam, P. K. D. V. Yarlagadda, *Proc. Inst. Mech. Eng., Part H* **2014**, *228*, 1083.
[7] A. P. Magiorakos, A. Srinivasan, R. B. Carey, Y. Carmeli, M. E. Falagas, C. G. Giske, S. Harbarth, J. F. Hindler, G. Kahlmeter, B. Olsson-Liljequist, D. L. Paterson, L. B. Rice, J. Stelling, M. J. Struelens, A. Vatopoulos, J. T. Weber, D. L. Monnet, *Clin. Microbiol. Infect.* **2012**, *18*, 268.
[8] K. S. Kaye, J. M. Pogue, *Pharmacotherapy* **2015**, *35*, 949.
[9] J. P. Pirnay, D. De Vos, L. Duinslaeger, P. Reper, C. Vandenvelde, P. Cornelis, A. Vanderkelen, *Crit. Care* **2000**, *4*, 255.
[10] M. R. Hemmila, A. Mattar, M. A. Taddonio, S. Arbabi, T. Hamouda, P. A. Ward, S. C. Wang, J. R. Baker, *Surgery* **2010**, *148*, 499.
[11] C. Henriquez-Camacho, G. Garcia-Casasola, C. Guillen-Astete, J. Losa, *J. Infect.* **2015**, *71*, 1.
[12] X. Pang, X. Liu, Y. Cheng, C. Zhang, E. Ren, C. Liu, Y. Zhang, J. Zhu, X. Y. Chen, G. Liu, *Adv. Mater.* **2019**, *31*, 1902530.
[13] L. L. Li, H. L. Ma, G. B. Qi, D. Zhang, F. Q. Yu, Z. Y. Hu, H. Wang, *Adv. Mater.* **2016**, *28*, 254.
[14] L. S. Xie, X. Pang, X. H. Yan, Q. X. Dai, H. R. Lin, J. Ye, Y. Cheng, Q. L. Zhao, X. Ma, X. Z. Zhang, G. Liu, X. Y. Chen, *ACS Nano* **2020**, *14*, 2880.
[15] S. Z. Lu, X. Y. Guo, M. S. Zou, Z. Q. Zheng, Y. C. Li, X. D. Li, L. L. Li, H. Wang, *Adv. Healthcare Mater.* **2020**, *9*, 1901229.
[16] Y. J. Li, X. X. Hu, D. Ding, Y. X. Zou, Y. T. Xu, X. W. Wang, Y. Zhang, L. Chen, Z. Chen, W. H. Tan, *Nat. Commun.* **2017**, *8*, 15653.
[17] L. L. Zhang, Y. Liu, Q. Y. Zhang, T. G. Li, M. Yang, Q. Q. Yao, X. L. Xie, H. Y. Hu, *Anal. Chem.* **2018**, *90*, 1934.
[18] M. L. Song, Y. Cheng, Y. Tian, C. C. Chu, C. Zhang, Z. X. Lu, X. Y. Chen, X. Pang, G. Liu, *Adv. Funct. Mater.* **2020**, *30*, 2003587.
[19] D. Wang, D. B. Cheng, L. Ji, L. J. Niu, X. H. Zhang, Y. Cong, R. H. Cao, L. Zhou, F. Bai, Z. Y. Qiao, H. Wang, *Biomaterials* **2021**, *264*, 120386.
[20] M. N. Pizzi, A. Roque, N. Fernandez-Hidalgo, H. Cuellar-Calabria, I. Ferreira-Gonzalez, M. T. Gonzalez-Alujas, G. Oristrell, L. Gracia-Sanchez, J. J. Gonzalez, J. Rodriguez-Palomares, M. Galinanes, O. Maisterra-Santos, D. Garcia-Dorado, J. Castell-Conesa, B. Almirante, S. Aguade-Bruix, P. Tornos, *Circulation* **2015**, *132*, 1113.
[21] F. Mota, A. A. Ordonez, G. Firth, C. A. Ruiz-Bedoya, M. T. Ma, S. K. Jain, *J. Med. Chem.* **2020**, *63*, 1964.
[22] R. Kumar, S. Basu, D. Torigian, V. Anand, H. Zhuang, A. Aavi, *Clin. Microbiol. Rev.* **2008**, *21*, 209.
[23] M. M. Welling, A. Bunschoten, J. Kuil, R. G. H. H. Nelissen, F. J. Beekman, T. Buckle, F. W. B. van Leeuwen, *Bioconjugate Chem.* **2015**, *26*, 839.
[24] X. H. Ning, S. Lee, Z. R. Wang, D. Kim, B. Stubblefield, E. Gilbert, N. Murthy, *Nat. Mater.* **2011**, *10*, 602.
[25] F. J. Hernandez, L. Y. Huang, M. E. Olson, K. M. Powers, L. I. Hernandez, D. K. Meyerholz, D. R. Thedens, M. A. Behlke, A. R. Horswill, J. O. McNamara, *Nat. Med.* **2014**, *20*, 301.
[26] H. Y. Chen, C. C. Liu, D. Chen, K. Madrid, S. W. Peng, X. Y. Dong, M. Zhang, Y. Q. Gu, *Mol. Pharmaceutics* **2015**, *12*, 2505.
[27] K. Ferreira, H. Y. Hu, V. Fetz, H. Prochnow, B. Rais, P. P. Muller, M. Bronstrup, *Angew. Chem., Int. Ed.* **2017**, *56*, 8272.
[28] N. Huang, X. Chen, X. F. Zhu, M. M. Xu, J. Liu, *Biomaterials* **2017**, *141*, 296.
[29] D. Mao, F. Hu, Kenry, S. L. J.i , W. B. Wu, D. Ding, D. L. Kong, B. Liu, *Adv. Mater.* **2018**, *30*, 1706831.
[30] M. M. Welling, C. M. de Korne, S. J. Spa, D. M. van Willigen, A. W. Hensbergen, A. Bunschoten, N. Duszenko, W. K. Smits, M. Roestenberg, F. W. B. van Leeuwent, *ACS Infect. Dis.* **2019**, *5*, 1160.
[31] V. Hoerr, C. Faber, *J. Pharm. Biomed. Anal.* **2014**, *93*, 136.
[32] C. N. Lee, Y. M. Wang, W. F. Lai, T. J. Chen, M. C. Yu, C. L. Fang, F. L. Yu, Y. H. Tsai, W. H. S. Chang, C. S. Zuo, P. F. Renshaw, *Clin. Microbiol. Infect.* **2012**, *18*, E149.
[33] C. H. Ren, H. M. Wang, X. L. Zhang, D. Ding, L. Wang, Z. M. Yang, *Chem. Commun.* **2014**, *50*, 3473.
[34] C. H. Yang, C. H. Ren, J. Zhou, J. J. Liu, Y. M. Zhang, F. Huang, D. Ding, B. Xu, J. Liu, *Angew. Chem., Int. Ed.* **2017**, *56*, 2356.
[35] J. H. Rao, I. J. Colton, G. M. Whitesides, *J. Am. Chem. Soc.* **1997**, *119*, 9336.
[36] P. Caravan, J. J. Ellison, T. J. McMurry, R. B. Lauffer, *Chem. Rev.* **1999**, *99*, 2293.
[37] S. Viswanathan, Z. Kovacs, K. N. Green, S. J. Ratnakar, A. D. Sherry, *Chem. Rev.* **2010**, *110*, 2960.
[38] R. Q. Yan, Y. X. Hu, F. Liu, S. X. Wei, D. Q. Fang, A. J. Shuhendler, H. Liu, H. Y. Chen, D. J. Ye, *J. Am. Chem. Soc.* **2019**, *141*, 10331.
[39] C. Y. Tong, L. Li, F. Xiao, J. L. Fan, X. H. Zhong, X. M. Liu, B. Liu, Z. H. Wu, J. Q. Zhou, *Biomater. Sci.* **2019**, *7*, 5097.
[40] U. N. Sundram, J. H. Griffin, T. I. Nicas, *J. Am. Chem. Soc.* **1996**, *118*, 13107.

 